Journal of Hydrology 612 (2022) 128299

Contents lists available at ScienceDirect

Journal of Hydrology

journal homepage: www.elsevier.com/locate/jhydrol

Research papers

Multi-objective optimization of aquifer storage and recovery operations under uncertainty via machine learning surrogates

Hamid Vahdat-Aboueshagh [a], Frank T.-C. Tsai [a,*], Emad Habib [b], T. Prabhakar Clement [c]

[a] Department of Civil and Environmental Engineering, Louisiana State University, Baton Rouge, LA 70803, USA
[b] Department of Civil Engineering & Institute for Coastal and Water Research, University of Louisiana at Lafayette, Lafayette, LA 70504, USA
[c] Department of Civil, Construction and Environmental Engineering, The University of Alabama, Tuscaloosa, AL 35487, USA

ARTICLE INFO

Keywords:
Aquifer storage and recovery
Multi-objective optimization
Surrogate modeling
Artificial neural network
Uncertainty analysis
Knee point of Pareto front

ABSTRACT

Aquifer storage and recovery (ASR) is an important water management approach to store excess surface water into aquifers for later use. Quantitative evaluation of ASR performance is not a trivial task and yet becomes more exacting when uncertainty analysis is added to the dimensionality of the problem. Inclusion of uncertainty into the framework of scheduling optimal ASR operations also increases the level of complexity. This study integrates a surrogate modeling approach coupled with a mixed integer nonlinear programming (MINLP) algorithm to optimize multi-objective ASR operations. The uncertainties are analyzed based upon a thorough sampling of the parameters space as well as a novel analysis of Pareto fronts and variograms of representative solutions. Knee point of representative Pareto fronts is selected for in-depth analysis. As a solution to the dimensionality of the problem, Artificial Neural Network (ANN) is employed to generate surrogate models for predicting groundwater levels and injectate distribution within the aquifer during ASR operations. The computational complexity in building a large number of ANNs and deriving of numerous Pareto fronts via solving the MINLP problem are overcome by the assistance of parallel computing. The results show that optimal ASR operations are highly influenced by hydraulic conductivity and longitudinal dispersivity. Higher hydraulic conductivity values lead to a higher number of active stress periods during storage and recovery phases, which requires large volume of extraction to recover the dispersed injectate. In contrast, higher ratios of longitudinal dispersivity to hydraulic conductivity adversely impact the injectate recovery efficiency. Through meaningful representation of objective function uncertainty by variograms, it is inferred that injectate recovery efficiency is more sensitive to longitudinal dispersivity than hydraulic conductivity.

1. Introduction

Aquifer storage and recovery (ASR) is an important water resource management method that can be used to store excess surface water into aquifers via artificial recharge (Forghani, 2018). The recharge can be accomplished by using various systems such as injection wells, infiltration basins and infiltration galleries that can use excess surface water, reclaimed water and stormwater, and water from other aquifers (Sheng, 2005; Dillon et al., 2009). There are two major phases in ASR operations: 1) storage phase, and 2) recovery phase. The ASR can be classified as a category of managed aquifer recharge (MAR) (Maliva, 2014). In ASR, the recharged water mixes with native water which is then extracted from aquifer during the recovery phase. During ASR, the storage phase (injection) is normally followed by the recovery phase (extraction). This study focuses on optimal scheduling of ASR operations where the storage and recovery phases are designed through injection of non-native water into the aquifer and subsequent extraction of stored groundwater from the aquifer using the same ASR well. Fig. 1 shows an ASR operation well installed in a confined aquifer. As shown in the figure, the process of water injection raises the groundwater level at the injection point and around the well. The groundwater raise leads to the development of an outward gradient from the ASR well. This mechanism can be used to develop hydraulic barriers that can force brackish/saline water away in aquifers (Shammas, 2008; Pyne, 2015). The rise in groundwater level can also help alleviate land subsidence in coastal areas where land loss is a core issue (Lu et al., 2011). In addition to

* Corresponding author.
E-mail addresses: hvahda1@lsu.edu (H. Vahdat-Aboueshagh), ftsai@lsu.edu (F.T.-C. Tsai), emad.habib@louisiana.edu (E. Habib), pclement@ua.edu (T.P. Clement).

https://doi.org/10.1016/j.jhydrol.2022.128299
Received 27 December 2021; Received in revised form 8 July 2022; Accepted 30 July 2022
Available online 6 August 2022

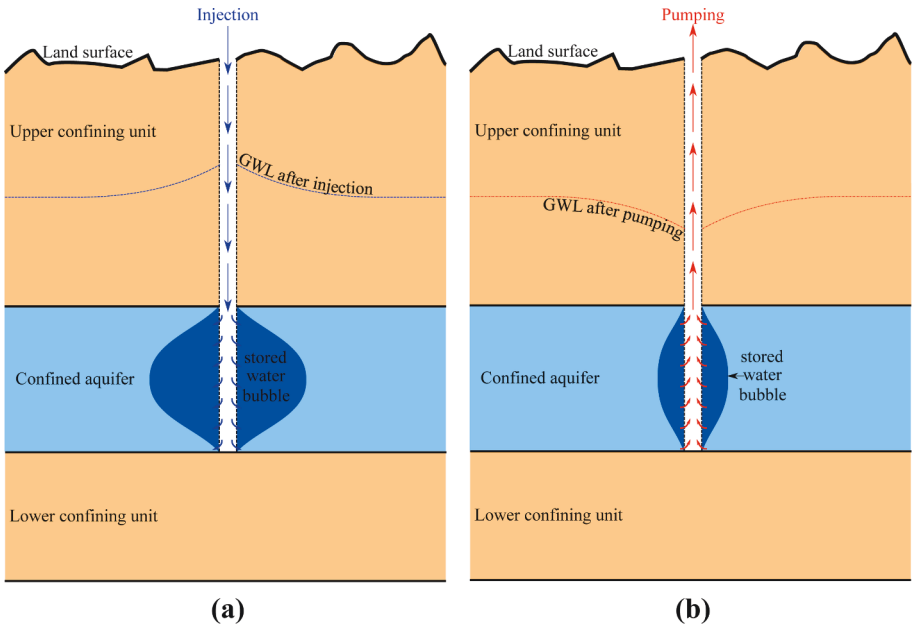

Fig. 1. A schematic of an ASR well for one ASR cycle in **(a)** storage phase, and **(b)** recovery phase. GWL: groundwater level in the confined aquifer.

acting as a hydraulic barrier, an ASR well can be used for storing surface water in aquifers during a wet season and the stored water can be later utilized during the dry season (Forghani and Peralta, 2017). There are other benefits from an ASR project such as agricultural water supply, restoration of groundwater levels, and reduction of environmental effects of streamflow diversions (Pyne, 1995; Khan et al., 2008).

Planning and design of ASR operations normally involve a sensitive balance between the amount of stored water and amount of withdrawn water considering the cost of various operations (Uddameri, 2007). There are many cost components to ASR operations which include capital costs and maintenance/operation costs (Almulla et al., 2005), and these costs may include the pumping cost, injection cost, and surface water treatment cost (Triki et al., 2019). The ASR operations may also be designed using multiple wells (Merritt, 1986). These wells could either be single-purpose wells, where water is solely injected into the aquifer or solely pumped out of the aquifer, or dual-purpose wells that are used for both injection and pumping (Zuurbier et al., 2014; Sultana et al., 2015). Although not the focus of this study, detrimental geochemical impacts of injectate and mobilization of contaminants in the receiving aquifer must be carefully considered during ASR operations (Sun et al., 2020; Fakhreddine et al., 2021). One of the operational aspects that has not received much attention is the scheduling of injection and pumping of these wells. The concept of an ASR cycle has been used for scheduling injection and pumping activities (Merritt, 1986). The performance of an ASR cycle can be quantitatively evaluated through the established concept of recovery efficiency (Lowry and Anderson, 2006; Ward et al., 2009; Lu et al., 2011; Guo et al., 2015; Forghani and Peralta, 2017). It is worth emphasizing that utilization of groundwater and transport models can facilitate measuring the ASR performance.

Recovery efficiency is the fraction of injected water (injectate) being extracted out of an aquifer during the pumping period. To calculate the recovery efficiency, injectate needs to be tracked during the ASR cycle. Solute transport models are normally coupled with groundwater flow models to track the injectate (Lowry and Anderson, 2006). A basic assumption employed in this approach is to assume a non-zero solute concentration for injectate while considering a zero concentration for native water in the aquifer (Forghani and Peralta, 2018). Previous studies have shown that the density effect (buoyancy effect) can be ignored as long as dispersive mixing is dominant and difference in density between injectate and native water is not large (Pavelic et al., 2006; Ward et al., 2007; Ward et al., 2009; Minsley et al., 2011). Hence, groundwater models with constant fluid density is suitable for most ASR operation assessments.

Hydrogeological parameters (such as hydraulic conductivity) in groundwater flow models and transport parameters (such as dispersivity) in solute transport models introduce uncertainty into recovery efficiency calculation. It is a common practice to generate realizations based on probability distribution of various parameters and conduct statistical analysis of model outputs for evaluating uncertainties (Fu and Gómez-Hernández, 2009; Refsgaard et al., 2012). Needless to say that including history matching techniques for estimating parameters significantly adds to computational burden of uncertainty quantification. In presence of all of these complexities, numerous runs of groundwater flow models and transport models become computationally expensive. Uncertainty quantification can become intractable without the aid of surrogate models, which mimics the behavior of flow and transport models (Keating et al., 2010; Razavi et al., 2012). Supervised artificial neural networks (ANN) have been demonstrated to be powerful surrogate models for groundwater flow and transport models (Yan and Minsker, 2006; Yan and Minsker, 2011; Luo and Lu, 2014). In addition to ANN models, deep learning approaches have shown promising results for flow and transport models (Chen et al., 2021a). The deep learning methods may also be utilized to generate subsurface structures in case of availability of sufficient data (Zhan et al., 2022). Due to robust and satisfying performance in groundwater and transport modeling, the ANN models were adopted as a machine learning method for prediction of groundwater levels and concentrations in this study (Nourani et al., 2008; Barzegar et al., 2017; Bedi et al., 2020).

This study introduces a supervised learning method with an evolutionary optimization algorithm to optimize ASR operations under parameter uncertainty. The objectives of an ASR operation are (1) to maximize the amount of injectate stored in the aquifer during the storage phase and (2) to maximize the recovery efficiency during the recovery phase. To demonstrate the results of this bi-objective optimization problem, where the objectives are conflicting, outcomes are represented on Pareto fronts, where a trade-off between objectives can be recognized (Reed et al., 2013; Reed and Kollat, 2013; Trindade et al., 2017; Akhtar and Shoemaker, 2019; Wang et al., 2022; Bau and Lee, 2011). Uncertainty of the Pareto front of the two objectives are investigated by considering uncertainties in hydraulic conductivity and

dispersivity. Other sources of uncertainties are not considered due to extensive computational requirements. To optimize ASR operations considering the uncertainties in these parameters, a supervised ANN method is employed as a substitute for the groundwater and the transport models.

This study is organized into six sections including this introduction section. Section 2 describes the mathematical methodologies including uncertainty assessment as well as the formulation of the optimization problem. Section 3 introduces the study area. Section 4 provides the specifics of the groundwater flow model, the transport model, the ANN models, and the optimization model. Section 5 discusses the results. Section 6 summarizes the key conclusions of this study.

2. Methodology

2.1. Formulation of ASR operation optimization

Performance of an ASR well is evaluated for an ASR cycle which includes one storage phase and one recovery phase. Each phase involves several individual pumping/injection stress periods. The storage phase starts at t_0 and ends at t_1. The recovery phase immediately follows the storage phase and ends at t_2. The injection rates are constrained between $I^{\min}$ and $I^{\max}$, and the pumping rates are constrained between $Q^{\min}$ and $Q^{\max}$. The ASR well is allowed to be inactive for certain periods where the injection/pumping rate is set to zero. The bi-objective ASR well operation optimization problem can be defined as:

$$\max \quad f_1 = \sum_{t=t_0}^{t_1} \Delta_t u_t I_t \tag{1}$$

$$\max \quad f_2 = \frac{\sum_{t=t_1}^{t_2} \Delta_t v_t Q_t C_t}{\sum_{t=t_0}^{t_1} \Delta_t u_t I_t C^0} \tag{2}$$

Subject to

$$I_t = \begin{cases} I_t, & \text{if } h_{t-1} < h^{\max} \\ 0, & \text{otherwise} \end{cases} \tag{3}$$

$$Q_t = \begin{cases} Q_t, & \text{if } h_{t-1} > h^{\min} \\ 0, & \text{otherwise} \end{cases} \tag{4}$$

$$I^{\min} \leqslant I_t \leqslant I^{\max} \tag{5}$$

$$Q^{\min} \leqslant Q_t \leqslant Q^{\max} \tag{6}$$

$$\sum_{t=t_0}^{t_1} u_t \geqslant 1 \quad \sum_{t=t_1}^{t_2} v_t \geqslant 1 \quad \forall u_t, v_t \in \{0,1\} \tag{7}$$

where Δ_t is the time interval of stress period t (day). I_t and Q_t denote the injection and pumping rates (m^3/day), respectively, during the stress period t. C_t is the concentration of injectate in the aquifer at the end of stress period t. C^0 is the initial injectate concentration. h_t is the groundwater level (m) at the end of stress period t. u_t and v_t are binary variables to indicate injection and pumping activeness, respectively. $u_t = 1$ indicates that injection occurs with injection rate I_t at stress period t. $v_t = 1$ indicates that pumping occurs with pumping rate Q_t at stress period t.

The first objective (Eq. (1)) maximizes the amount of injectate into the aquifer during the storage phase. The second objective (Eq. (2)) maximizes the injectate recovery efficiency during the recovery phase (Forghani and Peralta, 2018). The two objectives conflict with each other because f_1 is in the denominator of f_2. Eq. (3) and Eq. (4) are managerial constraints where the injection is not allowed when the groundwater level is above a threshold $h^{\max}$ and pumping is prohibited when the groundwater level is below a threshold $h^{\min}$. Eq. (5) and Eq. (6) are bound constraints for injection rates and pumping rates, respectively, when the pumps are active. Eq. (7) guarantees at least one active injection stress period and at least one active pumping stress period. Since ASR sites are typically small, this study assumes that the aquifer is homogeneous with respect to hydraulic conductivity and porosity.

The ASR operation optimization problem contains both continuous variables and binary variables. Consider the length of one ASR cycle to be a year with 12 monthly stress periods. The first 6 months are for the storage phase and the last 6 months are for the recovery phase as they resemble two natural phases of wet season and dry season in a year. There are 12 binary variables (u_t,v_t), by which the schedule is determined. There are also 12 continuous variables (I_t,Q_t), where the injection rates and pumping rates are assigned. The product of these binary and continuous variables results in injection rate or pumping rate for each stress period. Owing to the nonlinearity of the second objective function and groundwater level constraints, the optimization problem becomes a mixed integer nonlinear programming (MINLP) problem. The non-dominated sorting genetic algorithm (NSGA-II) (Deb et al., 2002) has been shown to be a promising approach for solving MINLP problems (Pasandideh et al., 2015; Rabbani et al., 2019; Chen et al., 2021b; Yin et al., 2020). The NSGA-II algorithm utilizes the standard GA processes and can be summarized in 6 steps: 1) population initialization, 2) non-dominated sorting, 3) crowding distance, 4) selection, 5) genetic operations (mutation and cross over), 6) and recombination and selection. Although the NSGA-II algorithm is selected for this study, other evolutionary methods, such as multi-objective particle swarm optimization (MOPSO), with outputs of non-dominated fronts can also be employed.

2.2. Uncertainty in model parameters and LHS sampling

It is well known that the optimal solutions to ASR operations will be impacted by various uncertainties that can include a wide range of model parameter and model structure uncertainties. This study specifically focuses on uncertainties in hydraulic conductivity values used in the groundwater flow equation and dispersivity values used in the solution transpose equation since the injectate plume is highly sensitive to these two model parameters.

This study adopts the Latin hypercube sampling (LHS) method to generate realizations of hydraulic conductivity and dispersivity values to address the uncertainty issues. Since the core to a successful Monte-Carlo simulation is the sampling method (Doucet et al., 2006), a better exploration of the parameter space would help perform a more thorough uncertainty assessment. Lack of a robust sampling method could introduce a computational curse (Janssen, 2013), where the computation time and the number of model runs for unnecessary sampled points hinder the progress. Stratified sampling, where different parts of a population is proportionally represented, is necessary for a thorough probe of the sample space (Neyman, 1992; Imbens and Lancaster, 1996). In this study, pairs of parameters for hydraulic conductivity and longitudinal dispersivity are generated based on Latin hypercube sampling (LHS), which is a stratified sampling approach (Iman and Conover, 1982; Helton and Davis, 2003). An LHS process for sampling two parameters is illustrated in the Supplementary Material Fig. S1.

2.3. Supervised learning-based surrogate modeling method

Calculating groundwater level h_t and concentration C_t at the end of each stress period for the ASR operation optimization problem can be intractable if the groundwater flow equation and solution transport equations are directly solved. This computational burden can be resolved by using surrogate models to efficiently produce groundwater levels and concentrations in the optimization framework. The application of ANN in groundwater and solute transport modeling has been well documented in Nourani et al. (2008), Barzegar et al. (2017), and Bedi et al. (2020). Prediction accuracy can be improved through adaptive

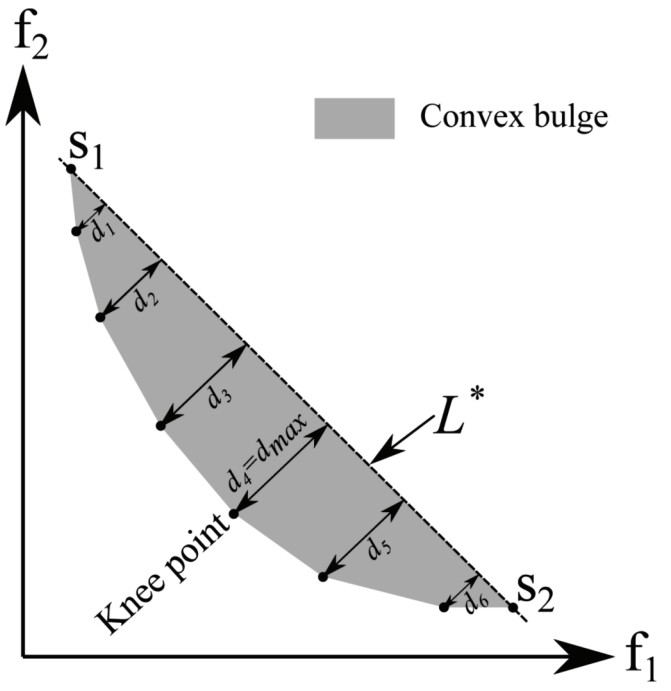

Fig. 2. Das characterization of knee point for a bi-objective Pareto front. The extreme line L^* passes through the extreme solution of s_1 with the lowest f_1 value and of s_2 with the lowest f_2 value on the Pareto front.

design-based surrogate modeling approach that adaptively combines the favorable characteristics of different surrogate models (Zhang et al., 2012).

2.4. Parameter and objective function uncertainties

To conduct in-depth uncertainty analysis, a representative solution for each Pareto front that is obtained by solving Eq. (1) to Eq. (7) for each set of parameters is selected in order to reduce computational requirements. Let Z be the number of Pareto fronts, which is equal to the number of discrete parameter pairs. At the first level, all the Pareto fronts are ranked to determine the representative fronts. At the end all the Pareto fronts will be ranked as the 1st, the 2nd, …, the Z^{th}. We name the 1st, the $(Z/2)^{th}$, and the Z^{th} Pareto fronts as the superior front, the median front, and the inferior front, respectively, and interpret them as representative Pareto fronts that cover the entire range of Pareto solutions. Analyzing entire Pareto fronts requires extensive computational resources. To determine the ranks of the Pareto fronts, the non-dominated sorting (Deb et al., 2002) is utilized. The ranking process is performed as follows:

I. Label the solutions of a given Pareto front in order to distinguish them from the rest of the Pareto fronts.
II. Run non-dominated sorting on the batch of all solutions of all Pareto fronts to obtain non-dominated solutions.
III. Determine the Pareto front with the most non-dominated solutions belonging to as the 1st rank Pareto front or the "superior front".
IV. By removing all solutions of the 1st rank Pareto front from the batch, repeat steps II and III to determine the 2nd rank Pareto front.
V. Repeat step IV to determine ranks for the 3rd, the 4th, …, the Z^{th} rank Pareto fronts.

At the second level, a representative solution is selected on each of the superior front, the median front, and the inferior front. The concept of the knee point, a point on non-dominated front for which a small gain in one objective costs a big loss on another objective, is applied to choose the representative solutions (Zhang et al., 2014; Ramirez-Atencia et al., 2017; Hamada and Chiba, 2017). There are optimization methods to identify the knee point based on the trade-off characteristics of the objective functions such as the hypervolume (Zhang et al., 2014), the sum of objectives (Rachmawati and Srinivasan, 2006), the proper utility (Shukla et al., 2013), and the angle-based knee point selection (Yue et al., 2017). This study utilizes Das characterization (Das, 1999) to identify the knee points of bi-objective Pareto fronts. The method is predicated upon calculation of distance between a given solution on Pareto front and the extreme line L^*, as shown in Fig. 2. The extreme line L^* passes through extreme solutions (s_1 and s_2) of a given Pareto front where f_1 and f_2 have their lowest values on the front. The basic assumption of the Das characterization is that the knee point corresponds to the maximum bulge (d_4) of the Pareto front.

As the final step, a sensitivity analysis at knee points is performed to find out how the ASR efficiency is affected through the parameter space for varieties of injection rates and pumping rates. The second objective function (f_2) is the target random function. In this study, sensitivity of the first objective is not of interest due to obvious relationship between the first objective function and hydraulic conductivity (K) and as longitudinal dispersivity (α_T) does not relate to the first objective function. The sensitivity of the second objective function to parameters at knee points is investigated through the variogram analysis of response surfaces (VARS) (Razavi and Gupta, 2016). K and α_T are the focused random variables for sensitivity analysis. In order to avoid the issue of incompatible rates of variability for different parameters and to have a unique range for which the impacts of different parameters can be compared with each other, the parameters are scaled within their maximum and minimum values (Razavi and Gupta, 2016). Hence, K and α_T are scaled by their upper and lower limits as $\overline{K} = (K - K_{\min})/(K_{\max} - K_{\min})$ and $\overline{\alpha}_T = (\alpha_T - \alpha_{T,\min})/(\alpha_{T,\max} - \alpha_{T,\min})$. By scaling so, the variograms (γ) of f_2 at distance lags $\Delta\overline{K}$ and $\Delta\overline{\alpha}_T$ are defined as:

$$\gamma(\Delta\overline{K}) = \frac{1}{2}\mathrm{E}[f_2(\overline{K} + \Delta\overline{K}) - f_2(\overline{K})]^2 \tag{8}$$

$$\gamma(\Delta\overline{\alpha}_L) = \frac{1}{2}\mathrm{E}[f_2(\overline{\alpha}_L + \Delta\overline{\alpha}_L) - f_2(\overline{\alpha}_L)]^2 \tag{9}$$

where E is the expectation operator. The variograms will show the variability of f_2 with respect to scaled lags of K and α_T, which indeed gives the flexibility of comparing f_2 with respect to variations of the two dimensionally different parameters.

3. Hypothetical ASR study site in Southwest Louisiana

Louisiana currently does not have an ASR site. However, the concept of ASR can be used to mitigate groundwater problems in Louisiana's coastal zone, which is routinely impacted by flooding and salinization. This study targets a potential ASR operation site based on the site selection suitability analysis for Southwest Louisiana conducted by LaHaye et al. (2021). The easy access to surface freshwater through local streams and suitable hydrogeologic characteristics of the underlying aquifer were the key criteria for selecting this potential ASR field demonstration site. The geochemical impacts of injected water could be investigated in future studies as water quality data become available. Fig. 3 shows the location of the study area in the north of Vermillion Parish, Louisiana. The model domain is 4 km by 4 km. The surface water source for the ASR operation may come from Bayou Grand Marais. The study area is covered by 27-meter thick clay layer at the top and is underlain by the thick undifferentiated sand of the Chicot aquifer system (Vahdat-Aboueshagh and Tsai, 2021). The undifferentiated sand is heavily pumped for agricultural purposes, and a large cone of depression has been created in the region (Fendick and Nyman, 1987; Lovelace et al., 2004). The adjacency to the Gulf of Mexico also makes this region prone to saltwater encroachment.

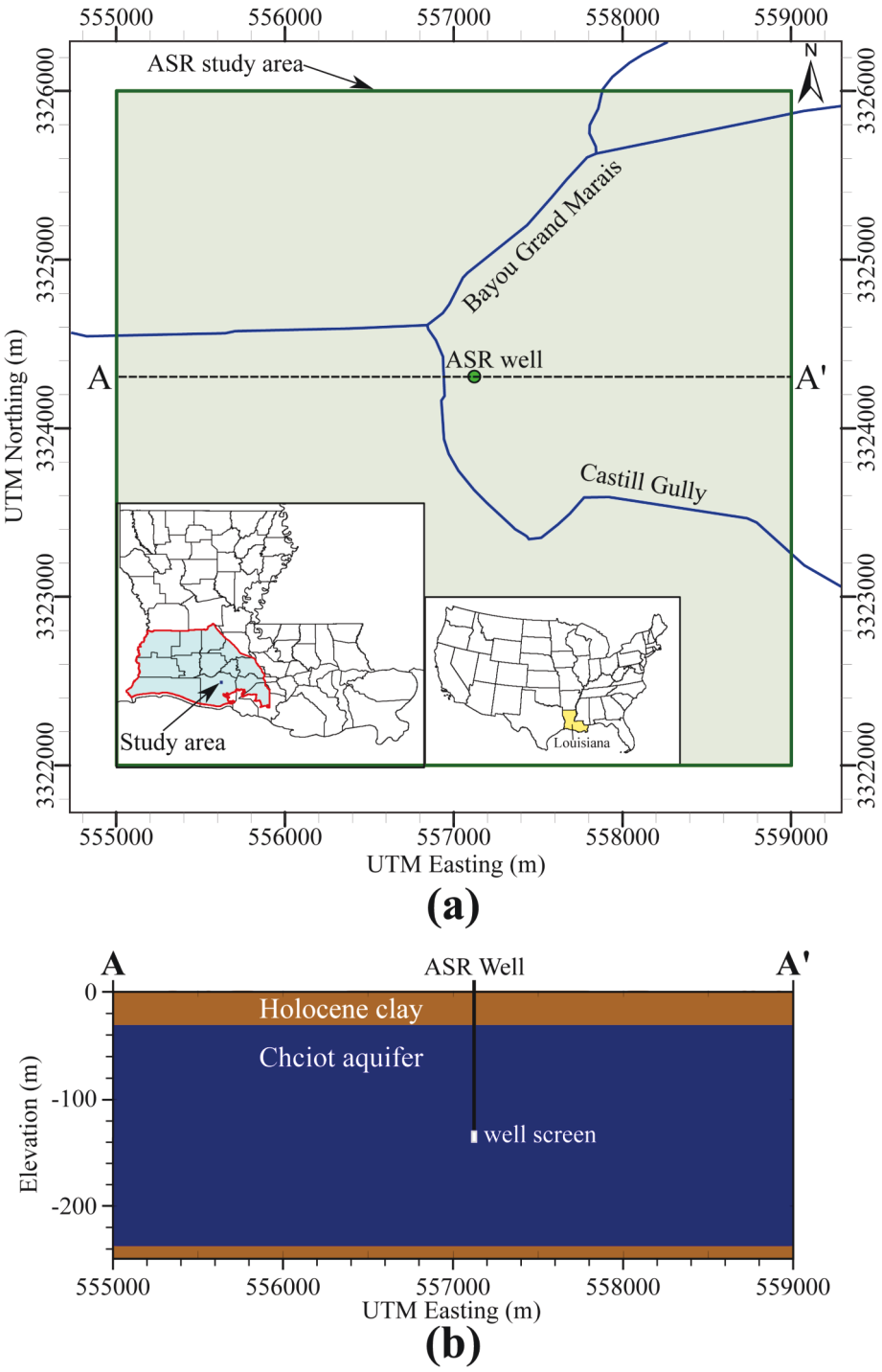

Fig. 3. The ASR study area. **(a)** The location of the ASR project area and a potential ASR well in the Chicot aquifer. **(b)** The Chicot aquifer along the AA' cross section. The coordinates are in NAD83/UTM zone 15 N.

4. Modeling setup

4.1. Groundwater flow model

A MODFLOW groundwater model (Harbaugh, 2005) for the study area was developed based on the hydrogeological information generated from a previously developed groundwater model (Vahdat-Aboueshagh et al. 2021). The model vertical extent is from land surface around 1 m down to −260 m NAVD 88. The horizontal cells size is 25 m. The model constitutes 24 layers with non-uniform thickness. The first layer and the last layer are confining layers. For the year 2015, the groundwater level of −9 m NAVD 88 was used as the constant-head boundary condition. The initial groundwater level was −8.70 m NAVD 88. 12 monthly stress periods were used for discretizing a one-year long ASR cycle. The ASR well screen was assumed to be from elevation of −129 m to −140 m NAVD 88.

Hydrogeologic properties of sand and clay were assumed to be homogeneous and isotropic. The specific storage and hydraulic conductivity values of sand are: 1.9×10^{-5} m^{-1} and 45.6 m/day, respectively (Vahdat-Aboueshagh et al. 2021). Previous studies suggested that natural logarithm of hydraulic conductivity, ln(*K*), for an aquifer follows a normal distribution (Benson, 1993; Yeh and Liu, 2000; Zhao and Illman,

Table 1
Data used in the simulation models, the ANN models and the optimization model.

Data	Value	Range
Model top, m	1	
Model bottom, m	−260	
Model area, m × m	4000 × 4000	
Number of model rows	160	
Number of model columns	160	
Number of model layers	24	
Screen location (row, column, layer)	(68,85,13)	
Log-hydraulic conductivity (lnK), m/day	3.82 (mean)	0.74 (standard deviation)
Specific storage, m^{-1}	1.9×10^{-5}	
Porosity	0.3	
Longitudinal dispersivity (α_L), m	50.025	0.05 – 100 (uniform)
α_H/α_L	0.1	
α_V/α_L	0.01	
Initial groundwater level, m	−8.70	
Boundary groundwater level, m	−9.00	
Number of injection stress periods	6	
Number of pumping stress periods	6	
C_0, mg/L	1000	
h_{min}, m	−10.70	
h_{max}, m	−6.70	
I_{min}, m^3/d	4000	
I_{max}, m^3/d	40,000	
Q_{min}, m^3/d	4000	
Q_{max}, m^3/d	40,000	
Number of pairs of (lnK,α_L)	100	
Number of ANN models	1800	
NSGA-II population size	120	
NSGA-II generation size	480	

2021). Vahdat-Aboueshagh et al. (2021) derived the mean and standard deviation for ln(*K*) to be 3.82 and 0.74, respectively, for the study site after appropriate model calibration. The porosity of the aquifer was assumed 0.3. Anisotropy and heterogeneity of hydraulic conductivity and porosity may have effects on the solutions and were not explored in this study. Future studies could assess these effects.

4.2. Transport model

This study employed the MT3DMS (Zheng and Wang, 1999) to track the injectate in the aquifer during the ASR cycle. To distinguish injectate from native groundwater, the injected water is assumed to contain an imaginary conservative solute (Forghani and Peralta, 2017) with concentration of 1000 mg/l. Probably the most challenging parameter in the contaminant transport models is the value of dispersivity (Burnett and Frind, 1987a; b). Due to our lack of knowledge about the nature of dispersive processes in groundwater systems (Frind et al., 1987), the longitudinal dispersivity is indeed an important uncertain parameter. In this study, the longitudinal dispersivity (α_L) is assumed to be a constant and assumed to follow a uniform probability distribution with a lower and an upper bound of 0.05 m and 100 m, respectively (Xu and Eckstein, 1995; Schulze-Makuch, 2005). Assuming lower values of the longitudinal dispersivity leads to sharp fronts with advection dominant behavior, while the higher values leads to mixed plumes having dispersion dominant behavior (Konikow, 2011). The horizontal transverse dispersivity (α_H) is assumed to be 0.1 of the longitudinal dispersivity and the ratio of vertical transverse dispersivity (α_V) to longitudinal dispersivity is assumed to be 0.01 (Zheng and Wang, 1999).

4.3. LHS sampling and model runs

In this study, 100 pairs of hydraulic conductivity and longitudinal dispersivity values were generated based on the LHS. Every pair was used to build a groundwater flow model and a solute transport model. Given a set of injection rates and pumping rates, the simulation models took approximately 5 min on a single core of the LSU SuperMike-II cluster to calculate groundwater level and concentration for 12 months.

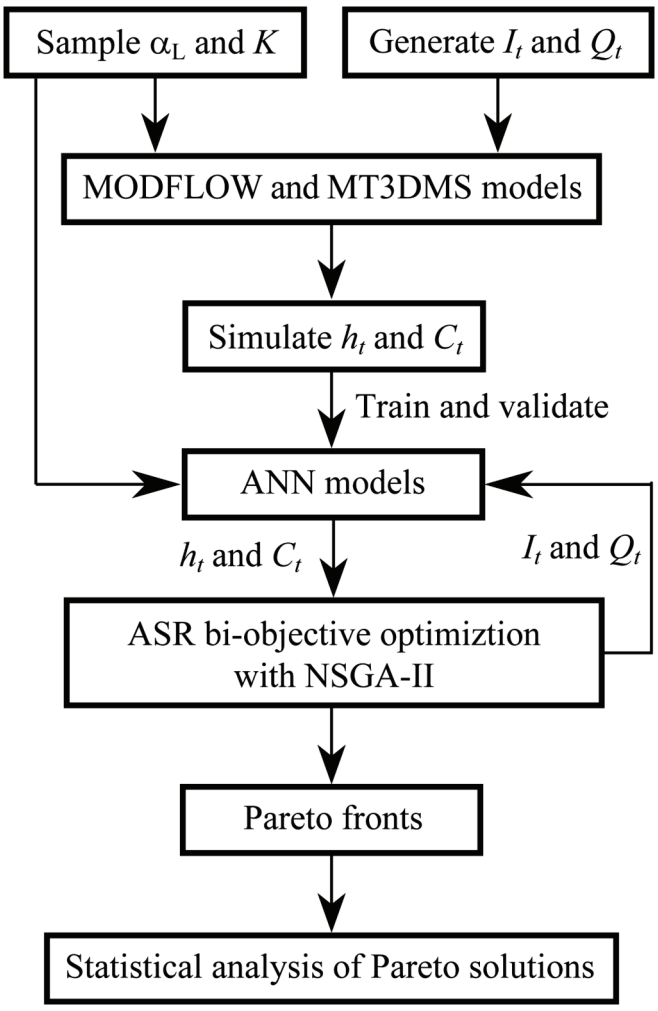

Fig. 4. Flowchart of methodology.

4.4. ANN models development with parallel computing

For 12 stress periods, 1000 random sets of injection rates and pumping rates (I_t and Q_t) together with 1000 random sets of binary values (u_t and v_t) were generated. The only consideration in sampling sets of u_t and v_t is the one shown in Eq. (7). These sets along with 100 generated pairs of hydraulic conductivity and longitudinal dispersivity were employed to train and validate ANN models for predicting groundwater levels and concentrations for 12 months in the ASR operation optimization problem. All of the 10^5 MODFLOW and MT3DMS models were run on 100 processers parallelly on the LSU SuperMike-II cluster. Each processor ran 1000 pairs of MODFLOW and MT3DMS models. The recorded groundwater levels from MODFLOW and concentrations from MT3DMS were input into ANN models.

We developed an ANN model for predicting groundwater level at the end of each stress period, and another ANN model for predicting concentration at the end of each pumping stress period. Therefore, there are a total of 1800 ANN models. A total of 100 parallel processors were utilized in parallel mode. Eighteen (18) ANN models were trained on each processor for predicting groundwater levels and concentrations for each pair of hydraulic conductivity and longitudinal dispersivity. All the ANNs are feedforward networks with a single hidden layer of 5 neurons. The training of the ANNs were performed in the parallel mode. The Levenberg-Marquardt (LM) algorithm was utilized to minimize the mean square error (MSE) cost function of the network (Ampazis and

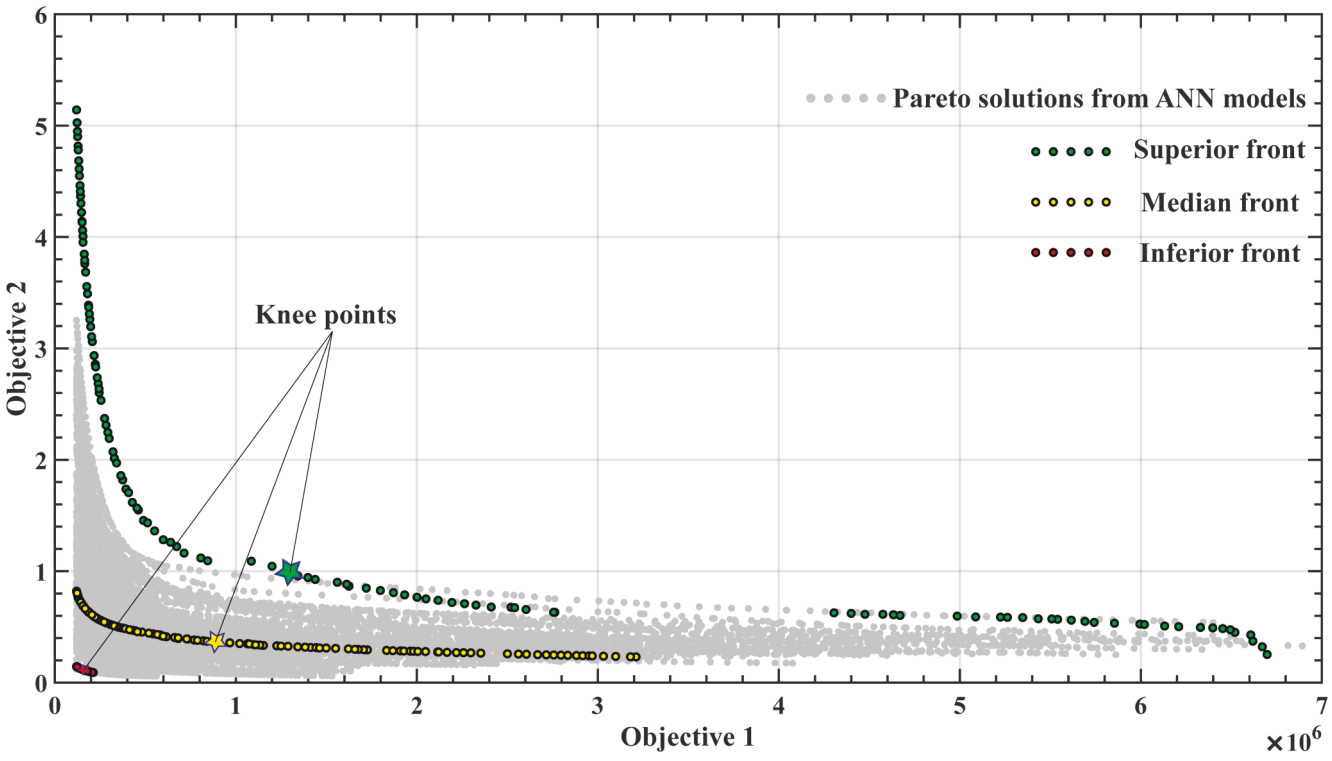

Fig. 5. Pareto solutions for the ASR operation optimization problem with uncertainties in hydraulic conductivity and longitudinal dispersivity values.

Perantonis, 2000; Singh et al., 2007).

The architectures of the ANN models were finalized through trial and error (Razavi et al., 2012). The proportions of training data, testing data, and validation data were determined as 70 %, 15 %, and 15 %, respectively, which are in accordance with the numbers reported in previous studies (Bowden et al., 2002; Shahin et al., 2004). The activation function of the hidden layer was set to the sigmoid function as it has been proved to be the best performer in capturing non-linearity of the modelled natural system (Nourani et al., 2008). The number of epochs was 928 on average for different models. The error average in groundwater level in different stress periods is less than 10^{-2} m in all the training, testing, and validation sets. The great performance of the ANN on groundwater level approximation has been reported frequently (Nourani et al., 2008; Trichakis et al., 2011). The error average in concentration in all the sets reduces continuously from 19 ml/l in the 7th stress period to 7 ml/l in the last stress period. The relatively higher concentration error in the 7th stress period is due probably to the complex behavior of the aquifer in transitioning from injection to pumping. However, the errors in concentration are all less than 2 %, which is satisfactory.

4.5. Optimization model with parallel computing

For each pair of hydraulic conductivity and longitudinal dispersivity values, the NSGA-II (Deb et al., 2002) was utilized to solve the bi-objective MINLP problem (Eq. (1)-Eq. (7)). The h_{max} and h_{min} were considered as 2 m above and 2 m below the initial groundwater head in the aquifer, respectively, which guarantees that the groundwater level will remain in the Holocene clay layer. The minimum injection rate and minimum pumping rate were set to 4,000 m^3/day (roughly 1 million gallon per day). The maximum injection rate and maximum pumping rate were set to 40,000 m^3/day (roughly 10 million gallon per day). The minimum and maximum rates were chosen based on pumping in the study region. The population size of 120 and generation size of 480 were set up for the NSGA-II. Parallel computations were performed to solve the 100 ASR optimization problems simultaneously. Table 1 lists the data used in the simulation models, the ANN models, and the optimization model. Fig. 4 shows the flowchart of methodology from sampling parameters, to developing MODFLOW/MT3DMS models, to training/validating ANN models, to solving the ASR operations optimization problem, and to analyzing Pareto solutions.

5. Results and discussion

5.1. Optimal solutions under uncertainty

The results of 100 Pareto fronts given 100 pairs of hydraulic conductivity and longitudinal dispersivity are shown in Fig. 5. The Pareto fronts with the 1st rank (the superior front), the 50th rank (the median front), and the 100th rank (the inferior front) and their knee points were determined and shown in the figure. The injectate amount (f_1) of Pareto fronts ranges between the minimum amount of 1.2×10^5 m^3 and 6.9×10^6 m^3 that is close to the maximum amount based on the upper limit (Eq. (5)). This means that almost the maximum amount of injection may be exploited in some parameter sets. The injectate recovery efficiency (f_2) varies between 0.1 and 5.1, which falls within the mathematical range of [0,6] for objective 2 based on the lower and upper limits (Eq. (5) and Eq. (6)). $f_2 > 1$ indicates that the amount of extraction is higher than the amount of injectate in order to achieve a higher recovery efficiency because of the injectate dispersion in the aquifer (Thomas et al., 2000). The diversity of the solutions of a Pareto front decreases as from the higher rank to the lower rank of Pareto fronts as the superior, median, and inferior fronts demonstrate. In other words, the higher the rank of a Pareto front, the more diverse the ASR scheduling becomes.

To further investigate the effect of the parameters on the Pareto fronts, Fig. 6a shows a general increasing trend in hydraulic conductivity (K) towards higher ranks of Pareto fronts. Since Pareto fronts with higher ranks have wider f_1 and f_2 values, Fig. 6a indicates that an aquifer with a higher hydraulic conductivity field can give broader ASR operation options because of lower fluctuations in groundwater level under higher injection and pumping rates. On the contrary, lower ratios of longitudinal dispersivity to hydraulic conductivity α_L/K (Fig. 6b) result

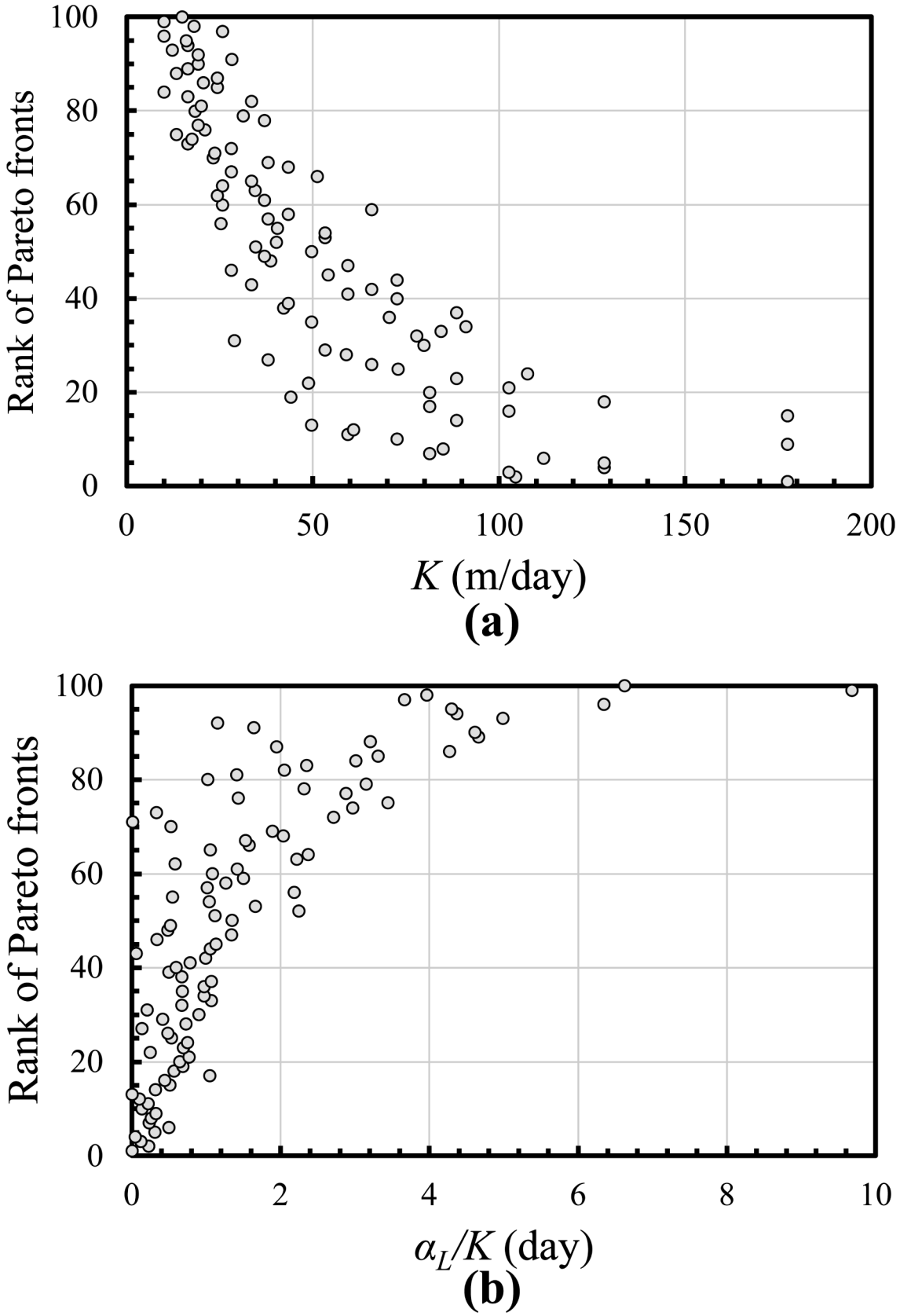

Fig. 6. Ranks of Pareto fronts with respect to parameters in the ASR operations optimization study **(a)** Rank versus hydraulic conductivity (K). **(b)** Rank against the ratio of longitudinal dispersivity to hydraulic conductivity (α/K).

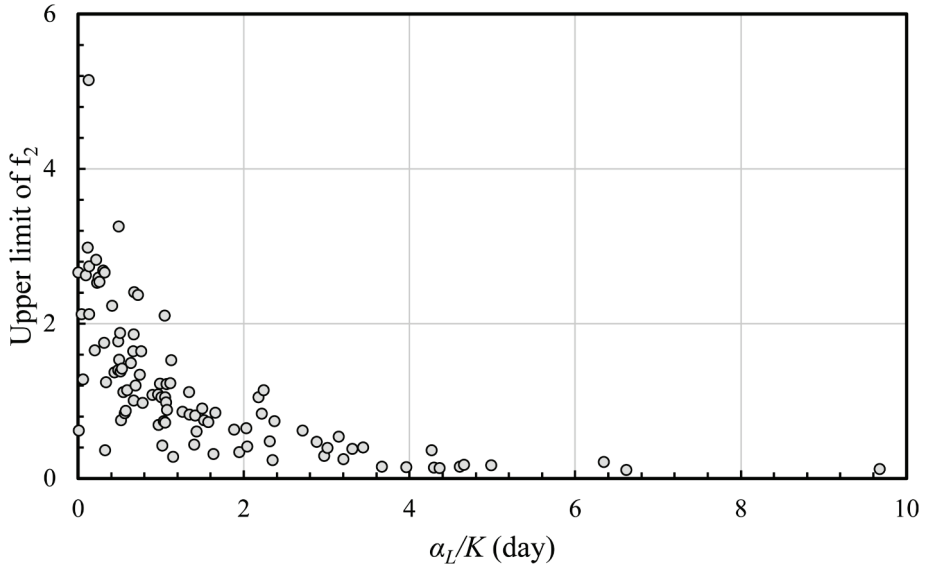

Fig. 7. Upper limit value of f_2 versus α_L/K for each Pareto front.

in Pareto solutions with higher ranks. The ratio α_L/K was chosen since it adequately represents the ratio of the injectate amount to the extraction amount in f_2 (Eq. (2)). High value of α_L/K implies lower values of K which leads to a lower amount of injectate (reduction in f_1) and lower pumping rates and leads to lower ranks of Pareto fronts. On the other hand, lower value of α_L corresponds to lower spread of injectate (smaller bubble) with high concentration (Ward et al., 2007), which leads to high ranks of Pareto fronts. To complement the analysis, the upper limit value of f_2 on each Pareto front with respect to corresponding α_L/K is shown in Fig. 7. This result is consistent with previous analyses that higher α_L/K tents to produce low-rank Pareto fronts, which have lower values of the upper limit of f_2. The upper limit of f_2 approaches 0 when $\alpha_L/K > 4$ day^{-1}.

5.2. Uncertainties in ASR scheduling

Fig. 8a shows the operation occurrence probability for each stress period. The operation occurrence refers to occurrence of either injection or pumping in a single stress period. The probability is the average of u_t or v_t for each stress period over 12,000 Pareto solutions. On average, the occurrence probability increases from 0.33 in the storage phase to 0.53 in the recovery phase indicating that the number of pumping operations is greater than the number of injection operations. In both phases the operation occurrence probability increases towards the end of the phase. The variation of the operation occurrence probability in the recovery phase is less than that in the storage phase. In other words, pumping occurrence is steadier throughout the entire recovery phase while injection occurrence is more likely near the end of the storage phase. The low injection occurrence probabilities in the 1st and the 2nd stress periods indicate high certainty that the beginning of the storage phase is not recommended to store water into the aquifer. In opposition, the pumping occurrence probabilities close to 0.5 in the 8th and the 9th stress periods indicate the most uncertain stress periods as scheduling pumping in those periods are less predictable.

The average injection rate and the average pumping rate for each stress period over the 12,000 Pareto solutions are provided in Fig. 8b. The similar pattern for the operation occurrence probability indicates that the higher the number of operations, the higher the volume of injectate or extraction. The average injection rate is 5,200 m^3/day and the average pumping rate is 7,200 m^3/day. This significant difference stems from the fact that injectate disperses in the aquifer as time passes (Thomas et al., 2000). Hence, more miscible water needs to be extracted to achieve a higher ASR efficiency.

The relationship between the hydraulic conductivity and the ASR schedule is also investigated as shown in Fig. 9. The steady increase of number of active stress periods as the values of K increases is consistent with the previous discussions that an aquifer with a higher hydraulic conductivity field can give broader ASR operation options. The percent of the Pareto solutions shows a decreasing trend as the number of active stress periods expands. More than 50 % of the Pareto solutions have less than 6 active stress periods and only less than 10 % of the Pareto solutions have more than 9 active stress periods. Further analysis of Pareto fronts obtained by the method in this study could be performed considering risk-tolerant or risk-averse polices in future studies (White et al., 2022).

The hydraulic conductivity also affects the amount of injectate and extracted water during ASR operations. Fig. 10 shows increasing average volumes of injection and extraction for every Pareto front with increasing hydraulic conductivity. The gap between the volumes of extracted water and injected water widens as the hydraulic conductivity increases due to higher dispersion of injectate. At higher hydraulic conductivity, the injectate travels further away from the ASR well, which allows higher injectate volumes and leads to a bigger stored bubble (Ward et al., 2007). Consequently, the wider bubble causes higher pumping rates in order to maximize the recovery (Lowry and Anderson, 2006).

5.3. Variation of groundwater level and concentration

Variation of groundwater levels at the ASR well across all the Pareto solutions in each stress period is shown in Fig. 11a. The last two stress periods (stress period 5 and 6) of the storage phase have the largest variation in groundwater level while the least groundwater level variation corresponds to the first two stress periods. These variations in groundwater level align with the probability of operation occurrence for stress periods explained in Fig. 8a. The recovery phase has relatively small groundwater level variation. Nevertheless, the range of groundwater level increases towards the end of the recovery phase.

Concentration and its variation at the ASR well in the recovery phase decrease with time as shown in Fig. 11b. Moreover, the maximum concentration of each stress period reduces monotonically from the beginning to the end of the recovery phase. The maximum concentration of the last stress period is 450 mg/l indicating that concentration at the ASR well is less than half of its initial concentration at the end of ASR

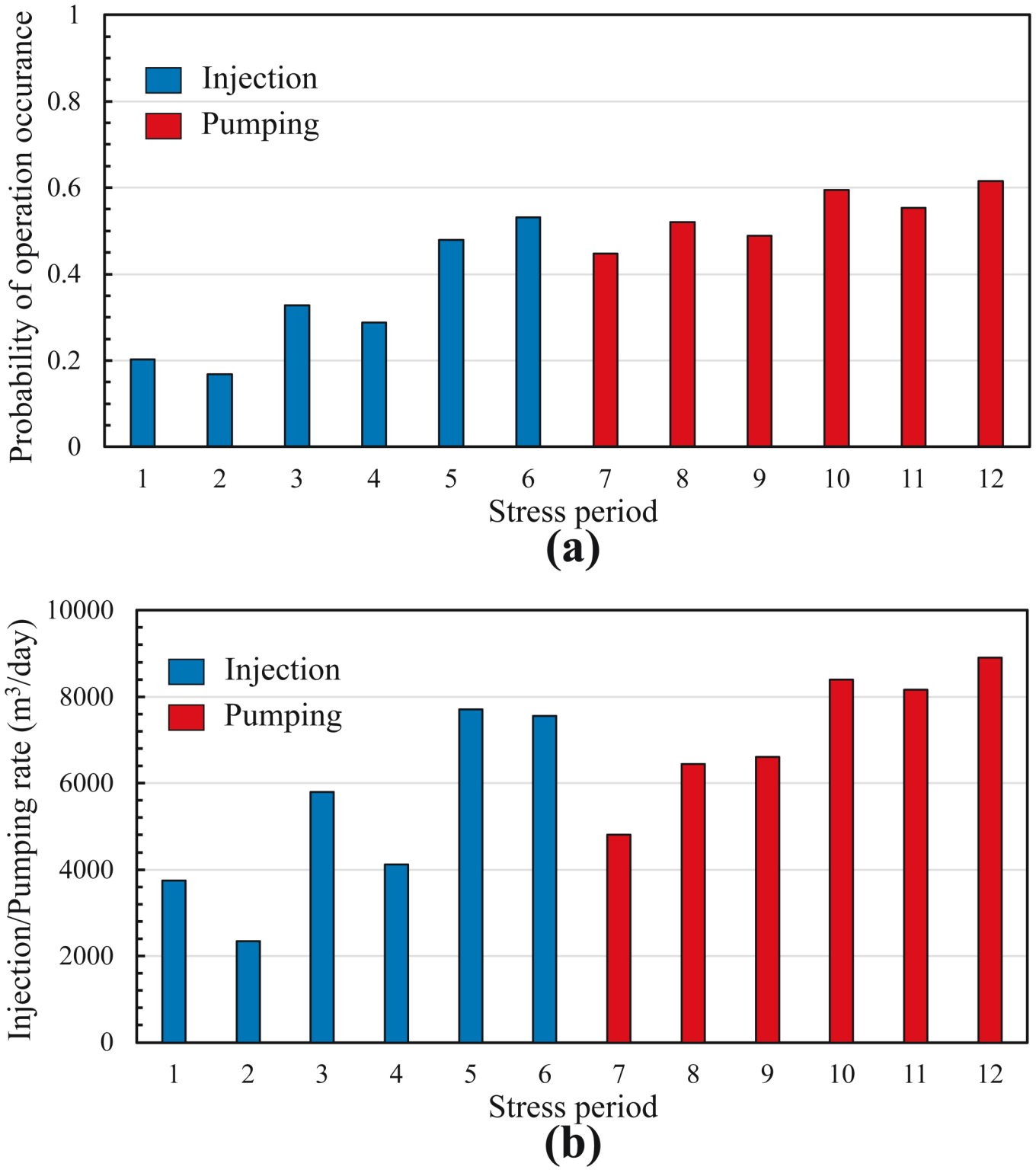

Fig. 8. Statistics of scheduling with respect to Pareto solutions. **(a)** Probability of ASR operation (injection or pumping) for each stress period. **(b)** Average amount of injection/pumping rate for each stress period.

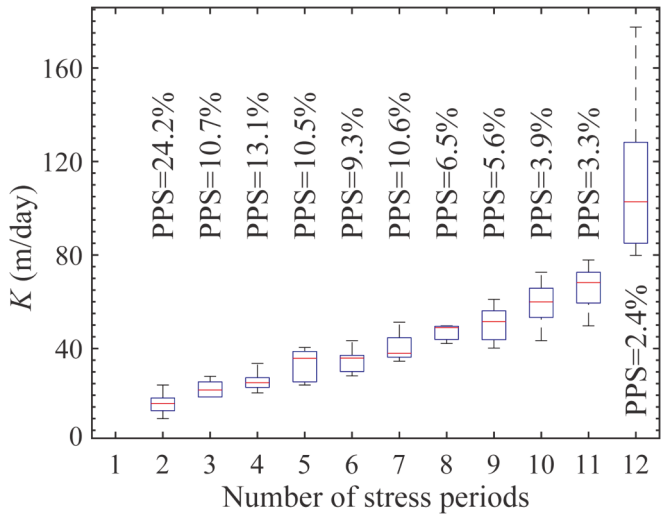

Fig. 9. Box plots of number of active stress periods (either $u_t = 1$ or $v_t = 1$) versus hydraulic conductivity of all Pareto solutions. PPS: Percent of Pareto solutions.

regardless of the scheduling and injection and pumping rates.

5.4. Variogram of f_2 at knee points

To extend the uncertainty analysis, the uncertainty of the second objective function (f_2) with respect to uncertainty K and α_L was expressed via variograms at the knee points of the superior front, median front, and inferior front as shown in Fig. 12. The values of K and α_L were uniformly sampled from their corresponding parameter ranges. The meaningful distance lag is up to 50 % of the parameter range (Razavi and Gupta, 2016). According to the variograms, α_L uncertainty has more effect on the f_2 uncertainty, compared to the effect of K uncertainty on the f_2 uncertainty in all three knee points. It is concluded that based on the given ranges of parameters, recovery efficiency is most sensitive to α_L.

6. Conclusions

This study formulates and solves a multi-objective MINLP optimization problem under uncertainty to optimally schedule operations for a one-year ASR operation cycle of injection and pumping. The incorporation of the ANN surrogate modeling into the MINLP shows promising results and very satisfying computational performance. Through analysis of the Pareto fronts, it was revealed that the efficiency of ASR is highly affected by the longitudinal dispersivity. Better performance of ASR in terms of the amount of injectate is achieved with higher values of hydraulic conductivity. Better performance of ASR in terms of injectate recovery efficiency is achieved with higher ratios of longitudinal dispersivity to hydraulic conductivity.

Investigating the schedule of ASR across Pareto solutions showed that injection near the end of the storage phase and pumping near the end of the recovery phase are likely to be robust policies. The pumping events tend to spread over the recovery phase while the injection events are mostly likely to occur at the end of the storage phase. The Pareto solutions for robust policies demonstrate that more than 50 % of the optimal solutions include a schedule with less than 6 active stress periods (either injection or pumping) over a 12-stress-period cycle. In robust policies, the volume of extracted water mostly exceeds the volume of injectate in optimal solutions and the gap between the volumes increases with higher values of hydraulic conductivity. This difference is attributable to the expansion of stored bubble with lower injectate concentration in aquifers with high hydraulic conductivity.

The analysis of the groundwater levels variation showed that the variation in the groundwater levels is the most at the end of injection period which is due to higher uncertainties associated with the end of the storage phase. The variation of injectate concentration diminishes with time through the recovery phase due to either pumping or dilution with the native groundwater.

The proposed method in this study can be applied to ASR scheduling problems with more than one cycle and may be researched in future

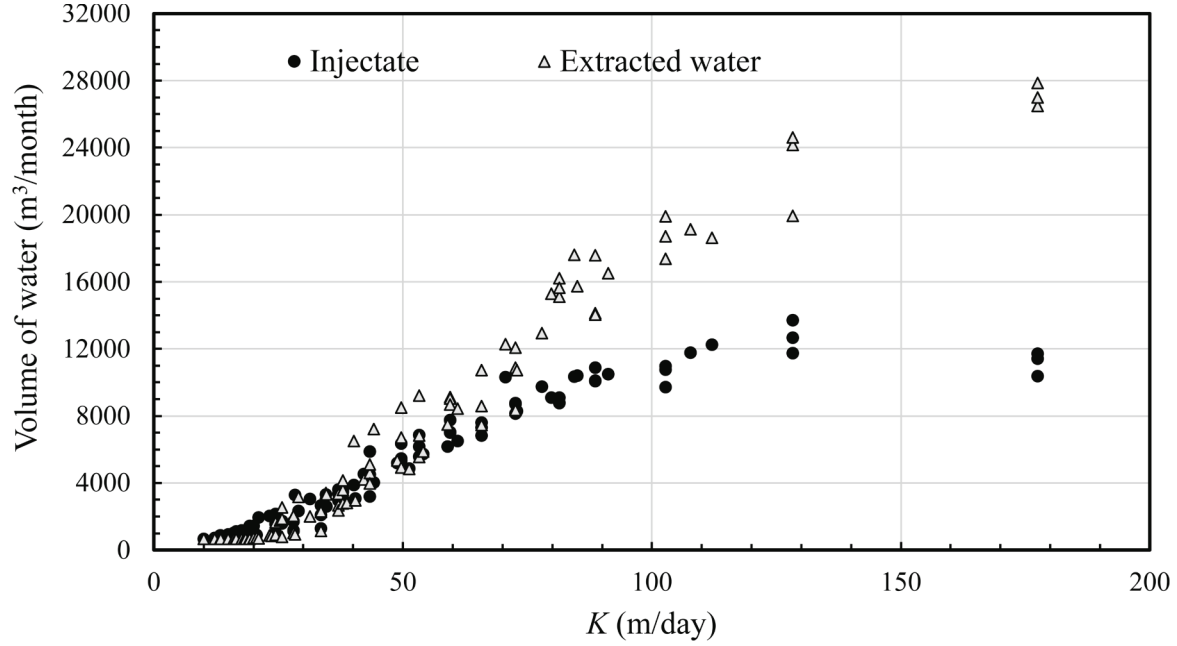

Fig. 10. Averaged volumes of injectate and extraction in each Pareto front.

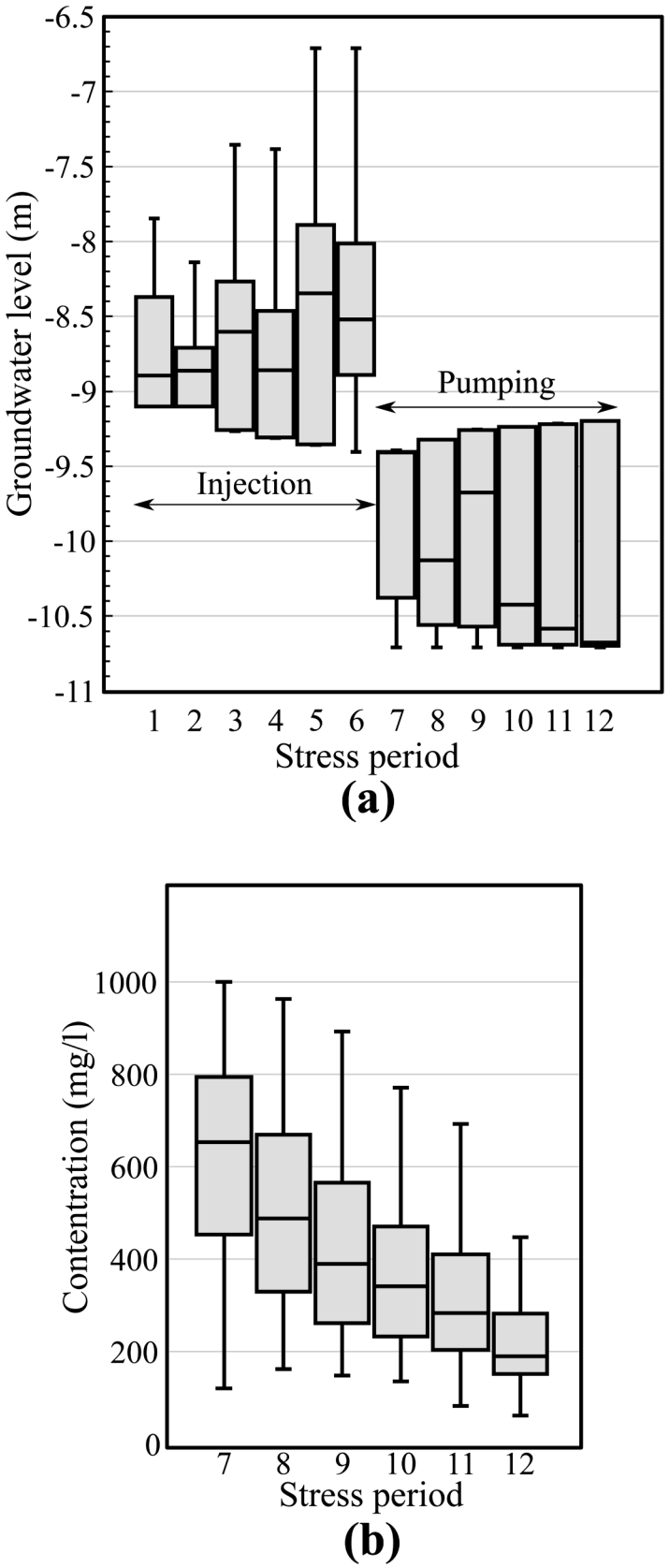

Fig. 11. **(a)** Box plots of groundwater level at the well, and **(b)** box plots of concentration at the well in the extraction period across the Pareto solutions.

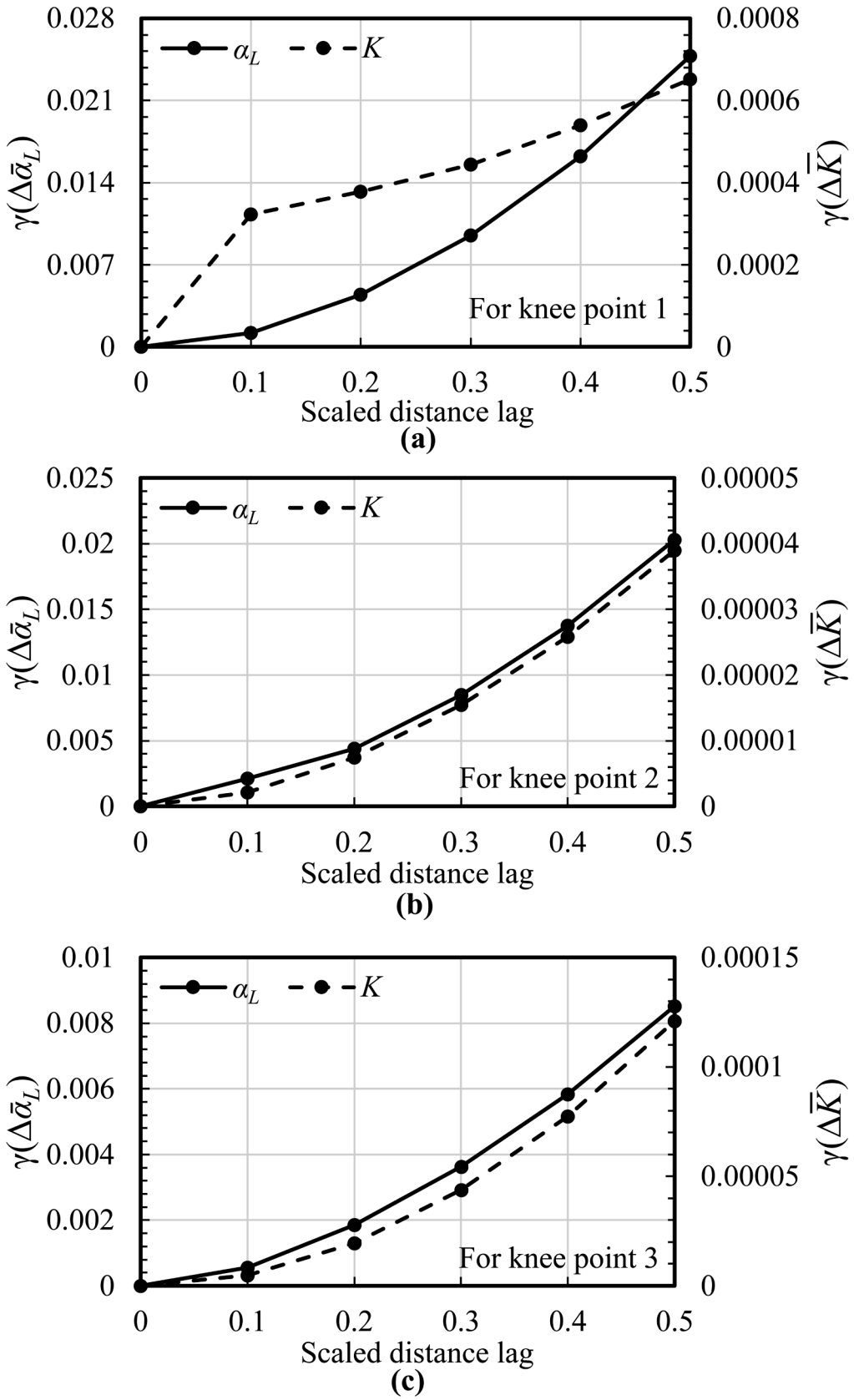

Fig. 12. Variograms for hydraulic conductivity (K) and longitudinal dispersivity (α) of **(a)** the representative solution on the superior front, **(b)** the representative solution on the median front, and **(c)** the representative solution on the inferior front.

studies.

CRediT authorship contribution statement

Hamid Vahdat-Aboueshagh: Conceptualization, Methodology, Software, Validation, Formal analysis, Investigation, Visualization, Writing - original draft, Writing - review & editing. **Frank T.-C. Tsai:** Conceptualization, Methodology, Investigation, Resources, Data curation, Supervision, Project administration, Funding acquisition, Writing - original draft, Writing - review & editing. **Emad Habib:** Funding acquisition, Conceptualization, Writing - original draft, Writing - review & editing. **T. Prabhakar Clement:** Funding acquisition, Conceptualization, Writing - original draft, Writing - review & editing.

Declaration of Competing Interest

The authors declare that they have no known competing financial interests or personal relationships that could have appeared to influence the work reported in this paper.

Data availability

Data will be made available on request.

Acknowledgments

This study was funded in part by the Louisiana Sea Grant College Program under U.S. Department of Commerce, the National Oceanic and Atmospheric Administration Award NA18OAR4170098 and the U.S. National Science Foundation EPSCoR Track-2 Program (Award No. 2019561). The authors acknowledge the LSU High Performance Computing (HPC) for providing the project with supercomputer resources.

Appendix A. Supplementary data

Supplementary data to this article can be found online at https://doi.org/10.1016/j.jhydrol.2022.128299.

References

Akhtar, T., Shoemaker, C.A., 2019. Efficient multi-objective optimization through population-based parallel surrogate search. arXiv preprint arXiv:1903.02167. https://doi.org/10.48550/arXiv.1903.02167.

Almulla, A., Hamad, A., Gadalla, M., 2005. Aquifer storage and recovery (ASR): a strategic cost-effective facility to balance water production and demand for Sharjah. Desalination 174 (2), 193–204. https://doi.org/10.1016/j.desal.2004.08.042.

Ampazis, N., Perantonis, S. J., 2000. Levenberg-Marquardt algorithm with adaptive momentum for the efficient training of feedforward networks. In Proceedings of the IEEE-INNS-ENNS International Joint Conference on Neural Networks. IJCNN 2000. Neural Computing: New Challenges and Perspectives for the New Millennium, 1, pp. 126-131. DOI: 10.1109/IJCNN.2000.857825.

Barzegar, R., Asghari Moghaddam, A., Adamowski, J., Fijani, E., 2017. Comparison of machine learning models for predicting fluoride contamination in groundwater. Stoch. Env. Res. Risk Assess. 31 (10), 2705–2718. https://doi.org/10.1007/s00477-016-1338-z.

Bau, D.A., Lee, J., 2011. Multi-objective optimization for the design of groundwater supply systems under uncertain parameter distribution. Pacific J. Optim. 7 (3), 407–424.

Bedi, S., Samal, A., Ray, C., Snow, D., 2020. Comparative evaluation of machine learning models for groundwater quality assessment. Environ. Monit. Assess. 192 (12), 1–23. https://doi.org/10.1007/s10661-020-08695-3.

Benson, C.H., 1993. Probability distributions for hydraulic conductivity of compacted soil liners. J. Geotechn. Eng. 119 (3), 471–486. https://doi.org/10.1061/(ASCE)0733-9410(1993)119:3(471).

Bowden, G.J., Maier, H.R., Dandy, G.C., 2002. Optimal division of data for neural network models in water resources applications. Water Resour. Res. 38(2), pp.2-1. https://doi.org/10.1029/2001WR000266.

Burnett, R.D., Frind, E.O., 1987a. Simulation of contaminant transport in three dimensions: 1. The alternating direction Galerkin technique. Water Resour. Res. 23 (4), 683–694. https://doi.org/10.1029/WR023i004p00683.

Burnett, R.D., Frind, E.O., 1987b. Simulation of contaminant transport in three dimensions: 2. Dimensionality effects. Water Resour. Res. 23 (4), 695–705. https://doi.org/10.1029/WR023i004p00695.

Chen, J., Dai, Z., Yang, Z., Pan, Y., Zhang, X., Wu, J., Reza Soltanian, M., 2021a. An improved tandem neural network architecture for inverse modeling of multicomponent reactive transport in porous media. Water Resour. Res. 57 (12) https://doi.org/10.1029/2021WR030595 e2021WR030595.

Chen, Y.-H., Tsai, F.T.-C., Jafari, N.H., 2021b. Multi-objective optimization of relief well operations to improve levee safety. J. Geotech. Geoenviron. Eng. 147 (7) https://doi.org/10.1061/(ASCE)GT.1943-5606.0002532.

Das, I., 1999. On characterizing the "knee" of the Pareto curve based on normal-boundary intersection. Struct. Optim. 18 (2), 107–115. https://doi.org/10.1007/BF01195985.

Deb, K., Pratap, A., Agarwal, S., Meyarivan, T.A.M.T., 2002. A fast and elitist multiobjective genetic algorithm: NSGA-II. IEEE Trans. Evol. Comput. 6 (2), 182–197. https://doi.org/10.1109/4235.996017.

Dillon, P.J., Pavelic, P., Page, D., Beringen, H., Ward, J., 2009. Managed aquifer recharge. *An introduction waterlines report series*, *13*, pp.1-64.

Doucet, A., Briers, M., Sénécal, S., 2006. Efficient block sampling strategies for sequential Monte Carlo methods. J. Comput. Graphical Stat. 15 (3), 693–711. https://doi.org/10.1198/106186006X142744.

Fakhreddine, S., Prommer, H., Scanlon, B.R., Ying, S.C., Nicot, J.P., 2021. Mobilization of arsenic and other naturally occurring contaminants during managed aquifer recharge: a critical review. Environ. Sci. Technol. 55 (4), 2208–2223. https://doi.org/10.1021/acs.est.0c07492.

Fendick, R. B. Jr., Nyman, D. J. (1987). Louisiana ground-water map no. 1: potentiometric surface, 1985, and water-level changes, 1983-85, of the Chicot aquifer in southwestern Louisiana, Water-Resources Investigations Report 86-4348. US Geological Survey.

Forghani, A., 2018. "Simulation and Optimization Models to Evaluate Performance of Aquifer Storage and Recovery Wells in Fresh Water Aquifers" *All Graduate Theses and Dissertations*. 6933. .

Forghani, A., Peralta, R.C., 2017. Transport modeling and multivariate adaptive regression splines for evaluating performance of ASR systems in freshwater aquifers. J. Hydrol. 553, 540–548. https://doi.org/10.1016/j.jhydrol.2017.08.012.

Forghani, A., Peralta, R.C., 2018. Intelligent performance evaluation of aquifer storage and recovery systems in freshwater aquifers. J. Hydrol. 563, 599–608. https://doi.org/10.1016/j.jhydrol.2018.06.042.

Frind, E.O., Sudicky, E.A., Schellenberg, S.L., 1987. Micro-scale modelling in the study of plume evolution in heterogeneous media. Stochastic Hydrol. Hydraulics 1 (4), 263–279. https://doi.org/10.1007/BF01543098.

Fu, J., Gómez-Hernández, J.J., 2009. Uncertainty assessment and data worth in groundwater flow and mass transport modeling using a blocking Markov chain Monte Carlo method. J. Hydrol. 364 (3–4), 328–341. https://doi.org/10.1016/j.jhydrol.2008.11.014.

Guo, W., Coulibaly, K., Maliva, R.G., 2015. Simulated effects of aquifer heterogeneity on ASR system performance. Environ. Earth Sci. 73 (12), 7803–7809. https://doi.org/10.1007/s12665-014-3822-4.

Hamada, N., Chiba, K., 2017. Knee point analysis of many-objective Pareto fronts based on Reeb graph. In 2017 IEEE Congress on Evolutionary Computation (CEC) (pp. 1603-1612). IEEE. DOI: 10.1109/CEC.2017.7969494.

Harbaugh, A. W. (2005). "MODFLOW-2005, The U.S. Geological Survey Modular Ground-Water Model: the ground-water flow process," in: Modeling techniques, Book 6, section A, (Reston, VA US Geological Survey), 253. https://doi.org/10.3133/tm6A16.

Helton, J.C., Davis, F.J., 2003. Latin hypercube sampling and the propagation of uncertainty in analyses of complex systems. Reliab. Eng. Syst. Saf. 81 (1), 23–69. https://doi.org/10.1016/S0951-8320(03)00058-9.

Iman, R.L., Conover, W.J., 1982. A distribution-free approach to inducing rank correlation among input variables. Commun. Stat.-Simul. Comput. 11 (3), 311–334. https://doi.org/10.1080/03610918208812265.

Imbens, G.W., Lancaster, T., 1996. Efficient estimation and stratified sampling. J. Econometrics 74 (2), 289–318. https://doi.org/10.1016/0304-4076(95)01756-9.

Janssen, H., 2013. Monte-Carlo based uncertainty analysis: sampling efficiency and sampling convergence. Reliab. Eng. Syst. Saf. 109, 123–132. https://doi.org/10.1016/j.ress.2012.08.003.

Keating, E.H., Doherty, J., Vrugt, J.A., Kang, Q., 2010. Optimization and uncertainty assessment of strongly nonlinear groundwater models with high parameter dimensionality. Water Resour. Res. 46 (10) https://doi.org/10.1029/2009WR008584.

Khan, S., Mushtaq, S., Hanjra, M.A., Schaeffer, J., 2008. Estimating potential costs and gains from an aquifer storage and recovery program in Australia. Agric. Water Manag. 95 (4), 477–488. https://doi.org/10.1016/j.agwat.2007.12.002.

Konikow, L.F., 2011. The secret to successful solute-transport modeling. Groundwater 49 (2), 144–159. https://doi.org/10.1111/j.1745-6584.2010.00764.x.

LaHaye, O., Habib, E.H., Vahdat-Aboueshagh, H., Tsai, F.T.-C., Borrok, D., 2021. Assessment of aquifer storage and recovery feasibility using numerical modeling and geospatial analysis: application in Louisiana. JAWRA J. Am. Water Resour. Assoc. 57 (3), 505–526.

Lovelace, J.K., Jared, W., Fontenot, C., Paul, F. (2004). Withdrawals, water levels, and specific conductance in the Chicot aquifer system in southwestern Louisiana, 2000-03, Scientific Investigations Report 2004-5212. U.S. Geol. Survey. https://doi.org/10.3133/sir20045212.

Lowry, C.S., Anderson, M.P., 2006. An assessment of aquifer storage recovery using ground water flow models. Groundwater 44 (5), 661–667. https://doi.org/10.1111/j.1745-6584.2006.00237.x.

Lu, C., Du, P., Chen, Y., Luo, J., 2011. Recovery efficiency of aquifer storage and recovery (ASR) with mass transfer limitation. Water Resour. Res. 47 (8) https://doi.org/10.1029/2011WR010605.
Luo, J., Lu, W., 2014. Comparison of surrogate models with different methods in groundwater remediation process. J. Earth Syst. Sci. 123 (7), 1579–1589. https://doi.org/10.1007/s12040-014-0494-0.
Maliva, R.G., 2014. Economics of managed aquifer recharge. Water 6 (5), 1257–1279. https://doi.org/10.3390/w6051257.
Merritt, M.L., 1986. Recovering fresh water stored in saline limestone aquifers. Groundwater 24 (4), 516–529. https://doi.org/10.1111/j.1745-6584.1986.tb01031.x.
Minsley, B.J., Ajo-Franklin, J., Mukhopadhyay, A., Morgan, F.D., 2011. Hydrogeophysical methods for analyzing aquifer storage and recovery systems. Groundwater 49 (2), 250–269. https://doi.org/10.1111/j.1745-6584.2010.00676.x.
Neyman, J., 1992. On the two different aspects of the representative method: the method of stratified sampling and the method of purposive selection. In: Breakthroughs in Statistics. Springer, New York, NY, pp. 123–150. https://doi.org/10.1007/978-1-4612-4380-9_12.
Nourani, V., Mogaddam, A.A., Nadiri, A.O., 2008. An ANN-based model for spatiotemporal groundwater level forecasting. Hydrol. Processes: Int. J. 22 (26), 5054–5066. https://doi.org/10.1002/hyp.7129.
Pasandideh, S.H.R., Niaki, S.T.A., Asadi, K., 2015. Bi-objective optimization of a multi-product multi-period three-echelon supply chain problem under uncertain environments: NSGA-II and NRGA. Inf. Sci. 292, 57–74. https://doi.org/10.1016/j.ins.2014.08.068.
Pavelic, P., Dillon, P.J., Simmons, C.T., 2006. Multi-scale hydraulic characterization of a stratified aquifer used for ASR. Ground Water 44 (2), 155–164. https://doi.org/10.1111/j.1745-6584.2005.00135.x.
Pyne, R.D.G., 1995. Groundwater Recharge and Wells: A Guide to Aquifer Storage Recovery. Lewis Publishers, Boca Raton, FL.
Pyne, R.D.G., 2015. Aquifer storage recovery: an ASR solution to saltwater intrusion at Hilton Head Island, South Carolina, USA. Environ. Earth Sci. 73 (12), 7851–7859. https://doi.org/10.1007/s12665-014-3985-z.
Rabbani, M., Heidari, R., Yazdanparast, R., 2019. A stochastic multi-period industrial hazardous waste location-routing problem: integrating NSGA-II and Monte Carlo simulation. Eur. J. Oper. Res. 272 (3), 945–961. https://doi.org/10.1016/j.ejor.2018.07.024.
Rachmawati, L., Srinivasan, D., 2006. A multi-objective genetic algorithm with controllable convergence on knee regions. In 2006 IEEE International Conference on Evolutionary Computation, pp. 1916-1923. IEEE. doi: 10.1109/CEC.2006.1688541.
Ramirez-Atencia, C., Mostaghim, S., Camacho, D., 2017. A knee point based evolutionary multi-objective optimization for mission planning problems. In: In ProceedIngs of the Genetic and Evolutionary Computation Conference, pp. 1216–1223. https://doi.org/10.1145/3071178.3071319.
Razavi, S., Gupta, H.V., 2016. A new framework for comprehensive, robust, and efficient global sensitivity analysis: 1. Theory. Water Resour. Res. 52 (1), 423–439. https://doi.org/10.1002/2015WR017558.
Razavi, S., Tolson, B.A., Burn, D.H., 2012. Review of surrogate modeling in water resources. Water Resour. Res. 48 (7) https://doi.org/10.1029/2011WR011527.
Reed, P.M., Hadka, D., Herman, J.D., Kasprzyk, J.R., Kollat, J.B., 2013. Evolutionary multiobjective optimization in water resources: the past, present, and future. Adv. Water Resour. 51, 438–456. https://doi.org/10.1016/j.advwatres.2012.01.005.
Reed, P.M., Kollat, J.B., 2013. Visual analytics clarify the scalability and effectiveness of massively parallel many-objective optimization: a groundwater monitoring design example. Adv. Water Resour. 56, 1–13. https://doi.org/10.1016/j.advwatres.2013.01.011.
Refsgaard, J.C., Christensen, S., Sonnenborg, T.O., Seifert, D., Højberg, A.L., Troldborg, L., 2012. Review of strategies for handling geological uncertainty in groundwater flow and transport modeling. Adv. Water Resour. 36, 36–50. https://doi.org/10.1016/j.advwatres.2011.04.006.
Schulze-Makuch, D., 2005. Longitudinal dispersivity data and implications for scaling behavior. Groundwater 43 (3), 443–456. https://doi.org/10.1111/j.1745-6584.2005.0051.x.
Shahin, M.A., Maier, H.R., Jaksa, M.B., 2004. Data division for developing neural networks applied to geotechnical engineering. J. Comput. Civil Eng. 18 (2), 105–114. https://doi.org/10.1061/(ASCE)0887-3801(2004)18:2(105).
Shammas, M.I., 2008. The effectiveness of artificial recharge in combating seawater intrusion in Salalah coastal aquifer, Oman. Environ. Geol. 55 (1), 191–204. https://doi.org/10.1007/s00254-007-0975-4.
Sheng, Z., 2005. An aquifer storage and recovery system with reclaimed wastewater to preserve native groundwater resources in El Paso, Texas. J. Environ. Manage. 75 (4), 367–377. https://doi.org/10.1016/j.jenvman.2004.10.007.
Shukla, P.K., Braun, M.A., Schmeck, H., 2013. Theory and Algorithms for Finding Knees. In: Purshouse, R.C., Fleming, P.J., Fonseca, C.M., Greco, S., Shaw, J. (eds) Evolutionary Multi-Criterion Optimization. EMO 2013. Lecture Notes in Computer Science, vol 7811. Springer, Berlin, Heidelberg. https://doi.org/10.1007/978-3-642-37140-0_15.
Singh, V., Gupta, I., Gupta, H.O., 2007. ANN-based estimator for distillation using Levenberg–Marquardt approach. Eng. Appl. Artif. Intell. 20 (2), 249–259. https://doi.org/10.1016/j.engappai.2006.06.017.
Sultana, S., Ahmed, K.M., Mahtab-Ul-Alam, S.M., Hasan, M., Tuinhof, A., Ghosh, S.K., Rahman, M.S., Ravenscroft, P., Zheng, Y., 2015. Low-cost aquifer storage and recovery: implications for improving drinking water access for rural communities in coastal Bangladesh. J. Hydrol. Eng. 20 (3), B5014007. https://doi.org/10.1061/(ASCE)HE.1943-5584.0001100.
Sun, J., Donn, M.J., Gerber, P., Higginson, S., Siade, A.J., Schafer, D., Seibert, S., Prommer, H., 2020. Assessing and managing large-scale geochemical impacts from groundwater replenishment with highly treated reclaimed wastewater. Water Resour. Res. 56 (11) https://doi.org/10.1029/2020WR028066 e2020WR028066.
Thomas, J.M., McKay, W.A., Cole, E., Landmeyer, J.E., Bradley, P.M., 2000. The fate of haloacetic acids and trihalomethanes in an aquifer storage and recovery program, Las Vegas, Nevada. Groundwater 38 (4), 605–614. https://doi.org/10.1111/j.1745-6584.2000.tb00252.x.
Trichakis, I.C., Nikolos, I.K., Karatzas, G.P., 2011. Artificial neural network (ANN) based modeling for karstic groundwater level simulation. Water Resour. Manage. 25 (4), 1143–1152. https://doi.org/10.1007/s11269-010-9628-6.
Triki, C., Zekri, S., Al-Maktoumi, A., Bazargan-Lari, M.R., 2019. Optimal location of wells for storage and recovery of surplus desalinated water in coastal aquifers. Groundwater 58 (5), 831–841. https://doi.org/10.1111/gwat.12951.
Trindade, B.C., Reed, P.M., Herman, J.D., Zeff, H.B., Characklis, G.W., 2017. Reducing regional drought vulnerabilities and multi-city robustness conflicts using many-objective optimization under deep uncertainty. Adv. Water Resour. 104, 195–209. https://doi.org/10.1016/j.advwatres.2017.03.023.
Uddameri, V., 2007. A dynamic programming model for optimal planning of aquifer storage and recovery facility operations. Environ. Geol. 51 (6), 953–962. https://doi.org/10.1007/s00254-006-0458-z.
Vahdat-Aboueshagh, H., Tsai, F.T.-C., 2021. Constructing large-scale complex aquifer systems with big well log data: Louisiana model. Comput. Geosci. 148, 104687 https://doi.org/10.1016/j.cageo.2021.104687.
Vahdat-Aboueshagh, H., Tsai, F.T.-C., Bhatta, D., Paudel, K.P., 2021. Irrigation-Intensive groundwater modeling of complex aquifer systems through integration of big geological data. Front. Water 3, 29. https://doi.org/10.3389/frwa.2021.623476.
Wang, W., Akhtar, T., Shoemaker, C.A., 2022. Integrating ε-dominance and RBF surrogate optimization for solving computationally expensive many-objective optimization problems. J. Global Optim. 82 (4), 965–992. https://doi.org/10.1007/s10898-021-01019-w.
Ward, J.D., Simmons, C.T., Dillon, P.J., 2007. A theoretical analysis of mixed convection in aquifer storage and recovery: how important are density effects? J. Hydrol. 343 (3–4), 169–186. https://doi.org/10.1016/j.jhydrol.2007.06.011.
Ward, J.D., Simmons, C.T., Dillon, P.J., Pavelic, P., 2009. Integrated assessment of lateral flow, density effects and dispersion in aquifer storage and recovery. J. Hydrol. 370 (1–4), 83–99. https://doi.org/10.1016/j.jhydrol.2009.02.055.
White, J.T., Knowling, M.J., Fienen, M.N., Siade, A., Rea, O., Martinez, G., 2022. A model-independent tool for evolutionary constrained multi-objective optimization under uncertainty. Environ. Modell. Software 149, 105316. https://doi.org/10.1016/j.envsoft.2022.105316.
Xu, M., Eckstein, Y., 1995. Use of weighted least-squares method in evaluation of the relationship between dispersivity and field scale. Groundwater 33 (6), 905–908. https://doi.org/10.1111/j.1745-6584.1995.tb00035.x.
Yan, S., Minsker, B., 2006. Optimal groundwater remediation design using an adaptive neural network genetic algorithm. Water Resour. Res. 42 (5) https://doi.org/10.1029/2005WR004303.
Yan, S., Minsker, B., 2011. Applying dynamic surrogate models in noisy genetic algorithms to optimize groundwater remediation designs. J. Water Resour. Plann. Manage. 137 (3), 284–292. https://doi.org/10.1061/(ASCE)WR.1943-5452.0000106.
Yeh, T.C.J., Liu, S., 2000. Hydraulic tomography: development of a new aquifer test method. Water Resour. Res. 36 (8), 2095–2105. https://doi.org/10.1029/2000WR900114.
Yin, J., Pham, H.V., Tsai, F.T.-C., 2020. Multi-objective spatial pumping optimization for groundwater management in a multi-aquifer system. J. Water Resour. Plann. Manage. 146 (4) https://doi.org/10.1061/(ASCE)WR.1943-5452.0001180.
Yue, C., Liang, J., Qu, B., Song, H., Li, G., Han, Y. (2017). A Knee Point Driven Particle Swarm Optimization Algorithm for Sparse Reconstruction. In: Shi, Y., et al. Simulated Evolution and Learning. SEAL 2017. Lecture Notes in Computer Science, vol 10593. Springer, Cham. https://doi.org/10.1007/978-3-319-68759-9_74.
Zhan, C., Dai, Z., Soltanian, M.R., Zhang, X., 2022. Stage-wise stochastic deep learning inversion framework for subsurface sedimentary structure identification. e2021GL095823 Geophys. Res. Lett. 49 (1).
Zhang, J., Chowdhury, S., Messac, A., 2012. An adaptive hybrid surrogate model. Struct. Multidiscip. Optim. 46 (2), 223–238. https://doi.org/10.1007/s00158-012-0764-x.
Zhang, X., Tian, Y., Jin, Y., 2014. A knee point-driven evolutionary algorithm for many-objective optimization. IEEE Trans. Evol. Comput. 19 (6), 761–776. https://doi.org/10.1109/TEVC.2014.2378512.
Zhao, Z., Illman, W.A., 2021. On the importance of considering specific storage heterogeneity in hydraulic tomography: laboratory sandbox and synthetic studies. J. Hydrol. 593, 125874 https://doi.org/10.1016/j.jhydrol.2020.125874.
Zheng, C., Wang, P.P., 1999. MT3DMS, A Modular Three-Dimensional Multispecies Transport Model for Simulation of Advection, Dispersion and Chemical Reactions of Contaminants in Groundwater Systems. Waterways Experiment Station, U.S. Army Corps of Engineers, Vicksburg, Mississippi.
Zuurbier, K.G., Zaadnoordijk, W.J., Stuyfzand, P.J., 2014. How multiple partially penetrating wells improve the freshwater recovery of coastal aquifer storage and recovery (ASR) systems: a field and modeling study. J. Hydrol. 509, 430–441. https://doi.org/10.1016/j.jhydrol.2013.11.057.